A NOVEL MARKER-LESS TUMOR TRACKING STRATEGY ON LOW-RANK FLUOROSCOPIC IMAGES FOR IMAGE-GUIDED LUNG CANCER RADIOTHERAPY

[1]*Wei Huang,* [1]*Jing Li,* [2]*Peng Zhang,* [3]*Min Wan*

[1]School of Information Engineering, Nanchang University, China
[2]School of Computer Science, Northwestern Polytechnical University, China
[3]National Heart Centre, SingHealth, Singapore

ABSTRACT

Fluoroscopic images recording the real-time motion of lung tumor lesion play an important role on lung cancer radiotherapy, as these images help to facilitate the accurate delivery of radiation dose on target tumor lesion. Derivation of tumor position in conventional lung tumor tracking strategies is realized via either placing external surrogates on patients or implanting internal fiducial markers in patients. Inaccurate tumor tracking and patient safety problems are often inevitable for these strategies. In this study, a novel marker-less tumor tracking strategy is presented for image-guided lung cancer radiotherapy. A fluoroscopic image is first decomposed into low-rank and sparse components based on robust-PCA via a split Bregman method. Then, a series of techniques, including K-means clustering, morphological processing, connected component analysis, etc are employed on obtained low-rank fluoroscopic images for tumor tracking. Clinical data obtained from 45 patients is incorporated for experimental evaluation. Promising results are demonstrated from the introduced strategy.

Index Terms— Mark-less Tumor Tracking, Fluoroscopic image, Robust-PCA, Split Bregman method, Image Processing

1. INTRODUCTION

Lung cancer is generally recognized as the most common cause of cancer-related death in worldwide population. According to [1], lung cancer is responsible for over 1.38 million deaths annually. Accurate diagnosis of lung cancer at its early stage and the timely treatment thereafter is essential to increase the survival time of patients, or even cure the disease [2]. There are various treatment manners for lung cancer to date, including surgery, radiotherapy, chemotherapy and palliative care [2], [3]. Among them, radiotherapy eliminating malignant cells via ionizing radiation is often essential in contemporary lung cancer treatment [2]. For lung cancer radiotherapy, precise prediction on positions of tumor lesion along with the respiratory cycle of patients is highly demanded, as high-dose-rate radiation beam needs to be concentrated on the tumor lesion and the radiation exposure towards its surrounding normal tissues should be kept as low as possible [2]. Conventional tumor tracking strategies in radiotherapy rely on markers including either external surrogates placed on the abdomen of patients [4] or internal fiducial markers implanted in patients [5]. However, their disadvantages are obvious: for external surrogates, it is often hard to correlate the movement between them and tumor lesion, resulting in lack of accuracy in tumor position derivation; for percutaneous marker implantation, patients are likely to suffer from the risk of pneumothorax. Therefore, marker-less tumor tracking strategies become more favored and necessary in lung tumor radiotherapy nowadays.

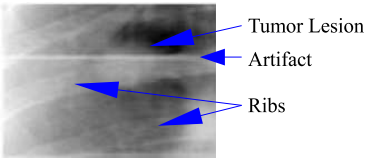

Fig. 1. Example of a fluoroscopic image.

Fluoroscopy, which is an effective and affordable medical imaging facility to obtain fluoroscopic image sequences about internal structures of patients, is widely incorporated in image-based lung cancer radiotherapy [6], [7], [8], [9]. In [6], regions-of-interest on image sequences containing discriminative tumor feature are shortlisted via a *principal component analysis* (PCA). In [7], nonlinear manifold learning methods, such as *locally linear embedding* (LLE), *local tangent space alignment* (LTSA), and *Laplacian eigenmap* (LAP), are incorporated similarly towards [6] but replacing the role of PCA for tumor position derivation. [8] and [9] utilize diverse popular pattern recognition tools including *artificial neural network* (ANN), *support vector machine* (SVM), linear/non-linear *regression* to accomplish the lung tumor tracking task on fluoroscopic images. For fluoroscopic images, the image quality is often poor caused by several factors (e.g. image noise

This work was supported by Programs No.20123BBG70208 and No.20123BBE50103 sponsored by Jiangxi Provincial Department of Science and Technology, as well as the National "863" Program No.2013AA013804.

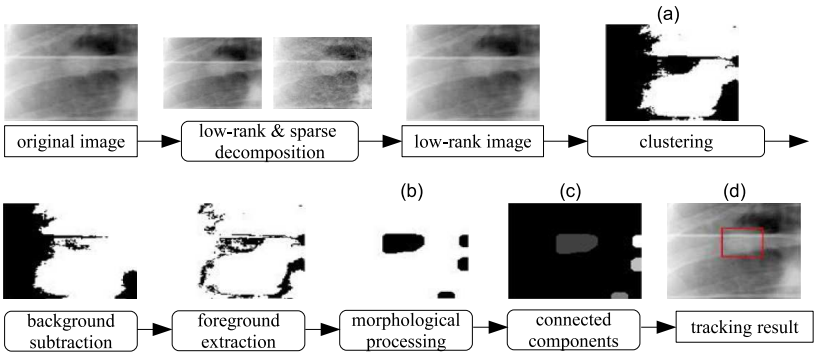

Fig. 2. Flowchart of the introduced marker-less lung tumor tracking strategy.

and artifact, patients' ribs occlusion obscuring the moving tumor lesion, etc). An example is illustrated in Fig.1. Also, non-tumor tissues surrounding the tumor lesion often move together with the tumor lesion within respiratory cycles, making it more challenging to differentiate tumor and localize its position precisely.

In this study, a novel marker-less tumor tracking strategy on fluoroscopic images for image-guided lung cancer radiotherapy is presented to tackle the above mentioned challenges. The flowchart of the strategy is depicted in Fig.2. A low-rank and sparse decomposition is applied on an original fluoroscopic image for the first time in this study. Obtained low-rank fluoroscopic images excluding major movement of non-tumor tissues are beneficial to provide clearer scenario about foreground (tumor) and background (non-tumor) for tumor tracking, which is realized via a series of pattern recognition and image processing techniques, including K-means clustering, morphological processing, connected component analysis, etc. Compared with other conventional marker-less lung tumor tracking studies, the main merit of the presented strategy resides in its simple implementation and relatively low computational cost. Costly manipulation (e.g. manifold learning in [7]) and training procedures (e.g. ANN, SVM, regression in [8], [9]), which are commonly seen in conventional mark-less lung tumor tracking studies, can be avoided in this presented tracking strategy. Therefore, the introduced strategy complies with the need of real-time tumor tracking in current clinical radiotherapy better.

The organization of the paper is as follows. In Section 2, a low-rank and sparse decomposition based on robust-PCA is introduced. After obtaining low-rank fluoroscopic images, Section 3 elaborates steps to track lung tumor lesion using a series of pattern recognition and image processing techniques. In Section 4, clinical data obtained from 45 patients are utilized to evaluate the performance of the introduced tumor tracking strategy. A compared strategy with the same tracking steps but directly applied on original fluoroscopic images are implemented to reveal the superiority of low-rank fluoroscopic images. In Section 5, the conclusion of this study is drawn.

2. LOW-RANK & SPARSE DECOMPOSITION ON FLUOROSCOPIC IMAGES

As introduced in Section 1, it is challenging to localize tumor lesion positions precisely on original fluoroscopic images, as the image quality is often poor and non-tumor tissues surrounding the tumor lesion also move, making the differentiation even harder. A general intuition to tackle this problem is that, the tumor tracking task should be more convenient to handle, if *an original fluoroscopic image χ can be decomposed into an image component χ_1 with major tumor movement over an ideal stationary background, as well as another image component χ_2 containing major non-tumor tissues movement*. Inspired by the recent prominent progress on robust-PCA [10], whose main idea is to recover a low-rank matrix A from a corrupted measurement D (i.e. $D = A + E$, where E denotes arbitrary error in magnitude and supposed to be sparsely supported [10]), such a low-rank and sparse decomposition in this tumor tracking study can be explicitly formulated via the following optimization problem:

$$\arg\min_{(\chi_1,\chi_2)} \|(\chi_1+\chi_2)-\chi\|_2^2 + \lambda_\star\|\chi_1\|_\star + \lambda\|\chi_2\|_1 \quad (1)$$

where $\|\cdot\|_1$, $\|\cdot\|_2$ and $\|\cdot\|_\star$ denote ℓ_1, ℓ_2, and nuclear norm, respectively; $\|\chi_1\|_\star$ penalizes the rank of χ_1 defined as the sum of its singular values with regularizing coefficient $\lambda_\star$; and $\|\chi_2\|_1$ is for promoting the sparsity of χ_2 with regularizing coefficient λ. In this study, a split Bregman method [11] is incorporated to solve the optimization problem in Eq.1. At each iteration k in the incorporated split Bregman method, Eq.1 can be solved via the following three steps:

Step 1: $\chi_1^k = \min_{\chi_1} \|(\chi_1+\chi_2^{k-1})-\chi^{k-1}\|_2^2 + \lambda_\star\|\chi_1\|_\star$ (2)

Step 2: $\chi_2^k = \min_{\chi_2} \|(\chi_1^k+\chi_2)-\chi^{k-1}\|_2^2 + \lambda\|\chi_2\|_1$ (3)

Step 3: $\chi^k = \chi^{k-1} - (\chi_1^k+\chi_2^k)$ (4)

For initialization (k=0), χ^0 is equivalent towards the original fluoroscopic image χ. At each iteration k, Step 1 can

be solved via a *singular value thresholding* (SVT) algorithm at a low computational cost. According to [11], the optimal solution of Step 2 can be rapidly obtained using a shrinkage operator $\chi_2^k = shrink(\chi^{k-1} - \chi_1^k, \frac{\lambda}{2})$. The whole iteration will terminate when $\|\chi_1^{k+1} - \chi_1^k\| \leq tol$, in which tol denotes an enough small change between two obtained low-rank fluoroscopic image χ_1 within two consecutive iterations. After all these steps are accomplished, a low-rank fluoroscopic image free of major movement of non-tumor tissues is produced. It will be utilized in the following tumor tracking process.

3. MARKER-LESS TUMOR TRACKING ON LOW-RANK FLUOROSCOPIC IMAGES

After obtaining a low-rank fluoroscopic image, clustering techniques can be applied on it directly (as illustrated in Fig.2(a)). The purpose of incorporating clustering here is to assign each pixel in the low-rank fluoroscopic image into different groups, so that pixels within the same group share similar visual attributes. In this study, we applied the well-known *K-means clustering* algorithm [12] to partition all pixels in the low-rank fluoroscopic image into two groups, i.e. tumor group and non-tumor group (K = 2 therein). Fig.2(a) includes one example of a binary image result after applying K-means clustering algorithm on a low-rank fluoroscopic image. Pixels with value of 1 (black) represent the tumor group, while pixels with value of 0 (white) belong to the non-tumor group.

It can be noticed that, although major moving non-tumor tissues surrounding tumor has already been identified and removed as the sparse fluoroscopic image χ_2 via Eq.1, some non-tumor tissues still exist after the clustering step, as their movement is not much and they are generally regarded as stationary background (i.e. low-rank fluoroscopic image χ_1 depicts tumor movement over stationary background according to Eq.1). Therefore, background subtraction and foreground extraction steps are necessary. In this study, since the movement of non-tumor tissues in low-rank fluoroscopic images is small, a background image is obtained via multiplication based on first few low-rank fluoroscopic images (after clustering) within the whole fluoroscopic image sequence of one patient. The foreground image excluding non-tumor tissues of less movement is extracted via the subtraction between obtained low-rank fluoroscopic images and their background image. The corresponding procedure is illustrated in Fig.3.

For foreground images extracted from low-rank fluoroscopic images, they are likely to be deteriorated by thin line structures and holes on tumor lesion, which are caused by image artifact and ribs occlusion, respectively. Hence, a morphological processing is applied on those foreground images to remove unnecessary fractions. The conducted morphological processing in this study is composed of an *opening* operation $f \circ s = (f \ominus s) \oplus s$ and a *closing* operation $f \bullet s = (f \oplus s) \ominus s$ [13], in which f indicates foreground images; s is a disk-shaped structuring element of radius 1 in this study; $\oplus$ and $\ominus$ represent dilation and erosion operations, respectively.

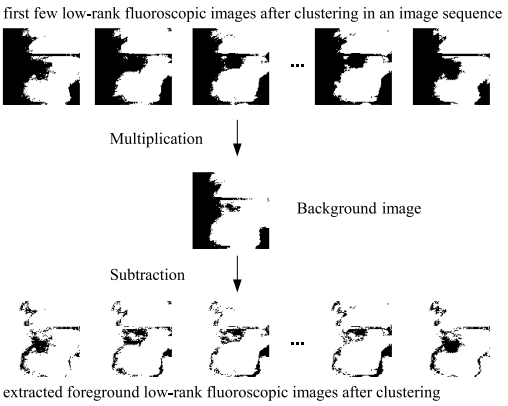

Fig. 3. An illustration of background subjection and foreground extraction in low-rank fluoroscopic images.

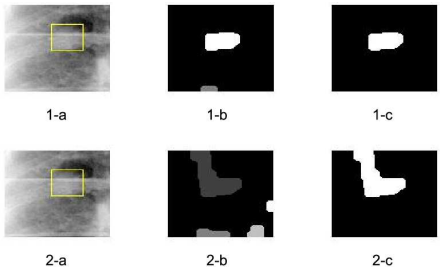

Fig. 4. An example of tumor tracking results on the same image data.

After morphological processing, several tumor lesion candidate regions are available (illustrated in Fig.2(b)). An automatic shortlisting approach here for target tumor lesion is via *connected component analysis* (CCA) [13]. CCA is capable to find uniquely labeled connected components on obtained image results after morphological processing (as shown in Fig.2(c), different candidate regions are labeled differently). After that, the target tumor lesion component is selected as the one with the highest spatial correlation with shortlisted tumor lesion in previous frames of the whole fluoroscopic image sequence, given the fact that tumor does not move rapidly frame by frame within respiratory cycles. After all these steps are performed, the tumor tracking result on one fluoroscopic image can be represented via a minimum rectangle enclosing the target tumor lesion region as illustrated in red in Fig.2(d).

4. EXPERIMENTS AND DISCUSSION

The performance of the introduced mark-less tumor tracking strategy has been evaluated by fluoroscopic image sequences obtained from 45 patients with lung tumor cancer. The av-

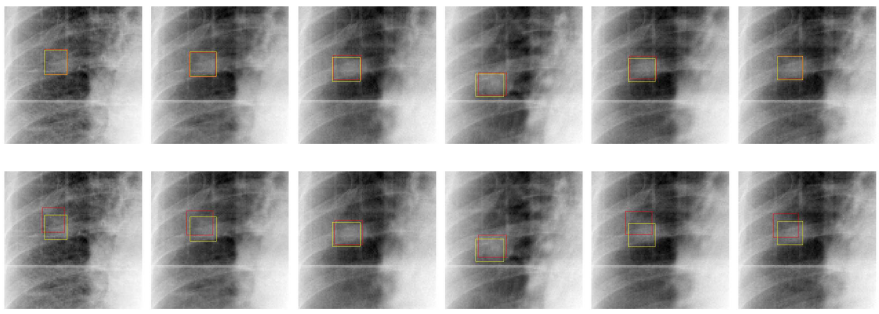

Fig. 5. Tracking results on example fluoroscopic images from the same patient within one respiratory cycle (from left to right) between the introduced strategy (1st row) and the compared strategy (2nd row). In each image, the yellow and red rectangle denotes the ground-truth and the tracking result of the tumor lesion, respectively.

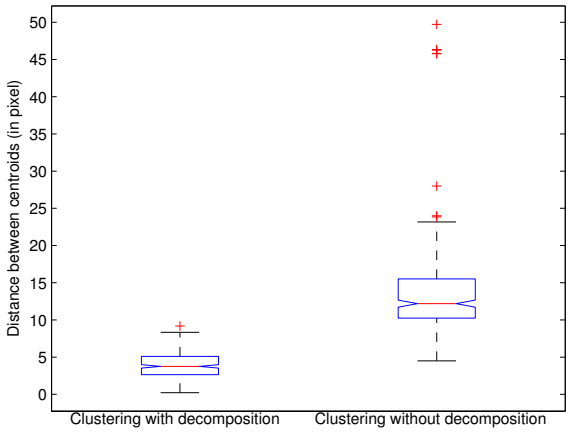

Fig. 6. Boxplot of distance between centroids on all experimental results.

erage duration of each image sequence is around 2 mins, in which 24 to 40 respiratory cycles are available. In order to demonstrate the superiority of low-rank fluoroscopic images in tumor tracking, the same tracking steps in Section 3 are implemented on original fluoroscopic images for comparison. An example of adopting two strategies on the same fluoroscopic image is illustrated in Fig.4. The first row represents the introduced strategy, while the second row is of the compared one. 1&2-a depict the same original fluoroscopic image with the same yellow rectangle enclosing the tumor lesion as its ground truth annotated by our senior clinicians. It can be observed that, results after morphological processing by the compared strategy is badly influenced by surrounding non-tumor tissues in the original fluoroscopic image (2-b), and its tracking result determined by the selected target tumor lesion after CCA will be deteriorated therein (2-c). For the introduced strategy, low-rank fluoroscopic images with less surrounding moving non-tumor tissues (1-b) can guarantee improved tracking results (1-c). Tumor tracking results in a respiratory cycle of one patient is depicted in Fig 5. It can be observed that tracking results via the newly introduced strategy are more accurate.

In order to quantitatively evaluate the tumor tracking performance, the distance between centroid of tracking results and that of ground truth is calculated on all tracking results. Based on those calculated results, a box-and-whisker plot is further generated in Fig 6. In each box, a red horizontal line is draw across each box representing the median, while upper and lower quartiles are depicted by blue lines above and below the median in each box. A vertical dashed line is drawn from the upper and lower quartiles to their most extreme data points, which are within a 1.5 *inter-quartile range* (IQR) [14]. Each data point beyond ends of a 1.5 IQR is marked by a plus symbol. It can be observed that, the box of the introduced strategy is significantly lower than that of the compared strategy, which indicates that low-rank fluoroscopic images have more precise tumor tracking performance (i.e. the median of centroids distance in the introduced strategy is around 4 pixels, compared with the over-10-pixel median of the compared strategy). Another important thing to observe is that, the 1.5 IQR of the introduced strategy is significantly shorter than that of the compared strategy, which suggests that the performance of the introduced tumor tracking strategy is more stable.

5. CONCLUSION

In this study, a novel marker-less tumor tracking strategy on low-rank fluoroscopic images for image-guided lung cancer radiotherapy is proposed. Promising results are demonstrated by applying the introduced strategy on real patient data. The main contribution of this study include incorporating low-rank and sparse decomposition for tumor tracking for the first time as well as a new corresponding tracking strategy based on the-first-time presented low-rank fluoroscopic images. Future studies will be continued with more sophisticated methods within the introduced tumor tracking framework.

6. REFERENCES

[1] J. Ferlay, H. Shin, and F. Bray, "Estimates of worldwide burden of cancer in 2008: Globocan 2008," *International Journal of Cancer*, vol. 127(12), pp. 2893–2917, 2010.

[2] C. Mountain, "Revisions in the international system for staging lung cancer," *Chest*, vol. 111(6), pp. 1710–1717, 1997.

[3] B. Ferrell, M. Koczywas, F. Grannis, and A. Harrington, "Palliative care in lung cancer," *Surgical Clinics of North America*, vol. 91(2), pp. 403–417, 2011.

[4] J. Hoisak, K. Sixel, R. Tirona, P. Cheung, and J. Pignol, "Correlation of lung tumor motion with external surrogate indicators of respiration," *International Journal of Radiation Oncology Biology Physics*, vol. 60(4), pp. 1298–1306, 2006.

[5] Y. Seppenwoolde, H. Shirato, K. Kitamura, S. Shimizu, M. van Herk, J. Lebesque, and K. Miyasaka, "Precise and real-time measurement of 3d tumor motion in lung due to breathing and heartbeat measured during radiotherapy," *International Journal of Radiation Oncology Biology Physics*, vol. 53(4), pp. 882–834, 2002.

[6] D. Ionascu, S. Park, J. Killoran, A. Allen, and R. Berbeco, "Application of principal component analysis for marker-less lung tumor tracking with beam's-eye-view epid images," *Medical Physics*, vol. 35(6), pp. 2893 (1 page), 2008.

[7] X. Li, H. Xu, S. Mukhopadhyay, N. Balakrishnan, A. Sawant, and P. Iyengar, "Toward more precise radiotherapy treatment of lung tumors," *IEEE Computer*, vol. 45(1), pp. 59–65, 2012.

[8] N. Riaz, P. Shanker, R. Wiersma, O. Gudmundsson, W. Mao, B. Widrow, and L. Xing, "Predicting respiratory tumor motion with multi-dimensional adaptive filters and support vector regression," *Physics in Medicine and Biology*, vol. 54(19), pp. 5735–5748, 2009.

[9] D. Ruan, J. Fessler, and J. Balter, "Real-time prediction of respiratory motion based on local regression methods," *Physics in Medicine and Biology*, vol. 52(23), pp. 7137–7152, 2007.

[10] E. Candes, X. Li, Y. Ma, and J. Wright, "Robust principal component analysis?," *Cornell University Library (arXiv.org)*, vol. 0912:3599, pp. 1–39, 2009.

[11] T. Goldstein and S. Osher, "The split bregman method for l1-regularized problems," *SIAM Journal of Imaging Sciences*, vol. 2(2), pp. 323–343, 2009.

[12] C. Bishop, *Pattern Recognition and Machine Learning*, Springer, 1st edition, 2007.

[13] R. Gonzalez and R. Woods, *Digital Image Processing*, Prentice Hall, 2nd edition, 2002.

[14] J. Rice, *Mathematical Statistics and Data Analysis*, Cengage Learning, 3rd edition, 2006.